Change in Rigidity in the Activated Form of the Glucose/Galactose Receptor from *Escherichia coli*: A Phenomenon that Will Be Key to the Development of Biosensors

Igor Sokolov,*† Venkatesh Subba-Rao,* and Linda A. Luck†
*Department of Physics, and †Department of Chemistry, Clarkson University, Potsdam, New York 13699

ABSTRACT Recently a periplasmic glucose/galactose binding protein, GGRQ26C, immobilized on a gold surface has been used as an active part of a glucose biosensor based on quartz microbalance technique. However the nature of the glucose detection was not clear. Here we have found that the receptor protein film immobilized on the gold surface increases its rigidity when glucose is added, which explains the unexpected detection signal. To study the rigidity change, we developed a new fast and simple method based on using atomic force microscopy (AFM) in tapping mode. The method was verified by explicit measurements of the Young's modulus of the protein film by conventional AFM methods. Since there are a host of receptors that undergo structural change when activated by ligand, AFM can play a key role in the development and/or optimization of biosensors based on rigidity changes in biomolecules.

INTRODUCTION

The potential use of periplasmic binding proteins as biosensors has arisen due to their solubility, stability, and ability to reversibly bind a large variety of small ligands including sugars, amino acids, and inorganic ions. These proteins comprise a large family of functionally similar receptors with a two-domain structure and a hinge cleft mechanism for binding substrate (1–4). Whereas the proteins are open and flexible when ligand is absent, they are more structurally compact and closed when ligand is bound (5,6). This large conformational change is the key to subsequent events in the chemotaxis pathways and transport of the bound substrates into the cytoplasm of the bacteria and can be used as a bioplatform for sensing small ligands (7–10). The most widely exploited receptor is the glucose/galactose binding protein (GGR), which binds D-glucose ($K_d = 0.2\ \mu M$) and D-galactose ($K_d = 0.4\ \mu M$) (11). This receptor is an ideal biomaterial since it is structurally and functionally well characterized. There are no disulfide bonds or free cysteine residues present in the native protein. However, a mutant of GGR (GGRQ26C) with an engineered single cysteine at amino acid 26 replacing a glutamine residue was utilized as a means to attach the protein to the gold surface via a covalent gold-sulfur bond for use in the biosensor experiments (12). In our quest for a glucose sensor, we have found that single cysteine mutants of the glucose/galactose binding protein can be immobilized on the gold surface. This film is capable of binding glucose. This binding event has been demonstrated by a number of techniques, including electrochemical impedance (13), surface plasmon resonance (14), and piezoelectric quartz crystal microbalance (QCM) (15).

The principle of the QCM technology is based on detecting the frequency decrease of the piezoelectric crystal resulting from mass changes on the surface when biomolecules are attached (16,17). Recently it has been shown that GGRQ26C directly attached to the gold surface of the QCM can be used as an effective glucose sensor even though the target sugars are predicted to be too low in mass to be detected (15). Applying the Voight model of a viscoelastic film to interpret the QCM data in the study indicated that the protein film should be considerably more viscous and/or possibly more rigid when glucose was bound. (18). Direct rigidity measurements shown in this study corroborate that hypothesis.

The atomic force microscopy (AFM) technique (19–21) is a natural choice to study mechanical properties of molecular films at the nanoscale. Several studies have been done on essentially atomically smooth surfaces (21–24). In the case of rougher surfaces, i.e., the gold surface of the piezoelectric crystal of the QCM, the inhomogeneity of the films can be considerable. Furthermore, the surface geometry should be measured to derive the Young's modulus, a geometry-independent characteristic of rigidity. Consequently, a large amount of statistical data is required to make conclusions about the mechanical properties of the film. Although these data can potentially be collected automatically (force-volume mode (25–27)), it still takes a considerable amount of time.

In this article, we suggest a simple and fast AFM method for detecting the rigidity change in protein film before and after addition of ligand. In this study we explicitly show that GGRQ26C protein film on a gold surface of the piezoelectric crystal indeed increases its rigidity when activated with glucose. To show consistency of this method with the more ''traditional'' direct measurements of rigidity (detecting not

Submitted February 3, 2005, and accepted for publication October 4, 2005.

Address reprint requests to Igor Sokolov, Dept. of Physics, Clarkson University, PO Box 5820, Potsdam, NY 13699-5820. Tel.: 315-268-2375; E-mail: sokolov@clarkson.edu.

0006-3495/06/02/1055/09 $2.00

doi: 10.1529/biophysj.105.060442

just the rigidity change), we explicitly measure the Young's modulus at a few points on the surface. The latter study shows both changes in rigidity and effective thickness of the surface layer that arises from ligand-induced conformational change of the protein.

This AFM method for detecting rigidity changes in proteins can be effective in the study and optimization of any sensors where the ligand-induced structural change occurs.

MATERIALS AND METHODS

Expression and purification of GGRQ26C

The GGRQ26C plasmid was expressed in *Escherichia coli* BL21 cells and purified as described previously by Carmon et al. (15). Protein was then dialyzed against two changes of 250 ml 3M guanidinium chloride (GnHCl), 100 mM KCl, 20 mM EDTA, 10 mM Tris pH 7.1, and four changes of 500 ml buffer containing 100 mM KCl, 10 mM Tris pH 7.1, and 0.5 mM $CaCl_2$. Quantitation of the protein was determined by extinction coefficient (ε_{280}) of 0.93 mL mg^{-1} cm^{-1} and an M_f of 33,370 (12).

Each molecule of GGRQ26C has a cysteine residue at position 26, which can be attached to a gold surface by a sulfur-gold covalent bond, as illustrated in Fig. 1. The size of each protein molecule of is $\sim 3.5 \times 6.5$ nm.

Protein immobilization on the gold surface of the piezoelectric crystal and subsequent activation by glucose

A piezoelectric quartz crystal used in the previously described QCM experiments (15) was used for the AFM experiments. This crystal was attached to a Petri dish by double-sided tape to prevent movement of the crystal during the measurements. The gold surface of the piezoelectric quartz crystal to which the protein was to be immobilized was first cleaned with ultraviolet short-wave light for 5 min. An AFM image of bare gold surface is shown in Fig. 2. One can see that the surface has granular structure. Despite that, the surface is rather flat. With the area of 3×3 μm^2, the height difference in the image is only 19 nm. It also can be quantified by roughness (RMS) parameter, which is equal here to ~ 2 nm.

A droplet (~ 500 μL) of 27 μM GGRQ26C protein in a buffer (100 mM KCl, 10 mM Tris pH 7.1, 0.5 mM $CaCl_2$) was then introduced to the gold surface. This solution incubated for 1 h in a closed Petri dish to ensure the formation of the gold-sulfur bond immobilizing the protein to the surface. Water was added around the glass slide to prevent possible evaporation of the buffer solution and drying of the protein surface. The immobilized protein surface was then washed with the above described buffer to reduce any nonspecific binding of the protein to the already immobilized protein or the gold surface. Specifically, the droplet was removed by tilting the slide, and ~ 2 mL of the buffer was added and then also removed by tilting.

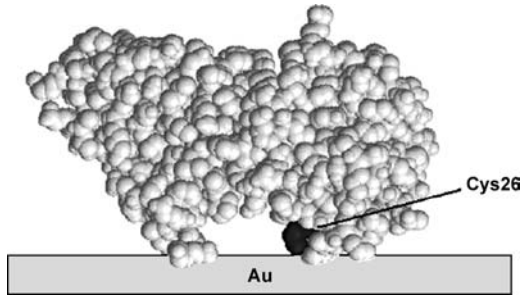

FIGURE 1 Space-filled depiction of GGRQ26C on the gold surface attached via a gold-sulfur bond to the cysteine residues at position 26. The protein is illustrated in the closed form with the ligand trapped in the cleft between the two domains.

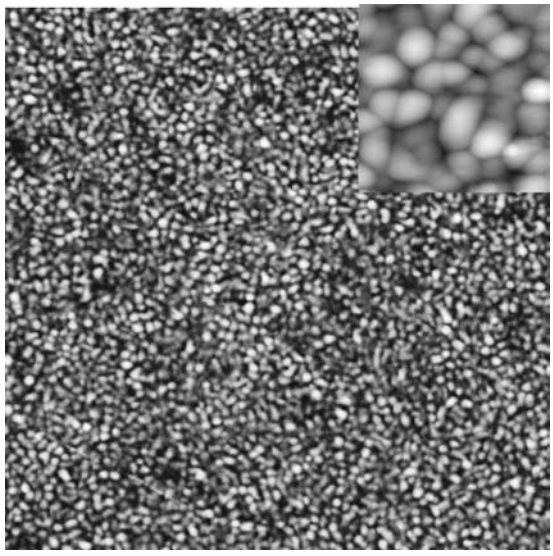

FIGURE 2 AFM scan of an area 3×3 μm^2; the height difference in the image is only 19 nm. The inset in the upper right corner is a close-up view of 350×350 nm^2.

The first AFM scanning experiments were performed in the buffer after this wash. The second AFM scans were done after adding glucose, as follows. Without disassembling the AFM liquid cell, 100 μL of 1 mM of glucose in the buffer was added to 2 mL buffer in the fluid cell, and left quiescent for 15 min before the start of scanning. Thus, the protein immobilized on the gold surface was exposed to ~ 50 μM glucose solution for 15 min. The surface was then rescanned by AFM.

Atomic force microscope

Dimension 3100 Nanoscope IIIa with an extender box, by Digital Instruments/Veeco (Santa Barbara, CA), was used in this study. The imaging was done in liquid using a standard fluid holder. There were two types of the AFM cantilevers used for the imaging in tapping mode. The first tip, tip 1 (FESP AFM cantilevers with silicon tip; Digital Instruments/Veeco), was used for tapping-mode scanning in liquid. The radius of the probe was tested on a 3-D tip characterization gratings (TGT1 by Micromash, Englewood, CO). A typical AFM tip used had an apex radius of ~ 10 nm. The driven oscillating amplitude was at 20 mV; the oscillating frequency in liquids was ~ 30 KHz. The second cantilever tip, tip 2, was a regular V-shaped silicon nitride cantilever with an integrated pyramidal tip (Digital Instruments/Veeco). The driving amplitude was set at 3 V, with an oscillating frequency of 6 Khz. Both tips were cleaned before each series of measurements by an ultraviolet short-wave lamp for 2 min. The scan rate was set at 0.5–1 Hz to optimize the image quality. Each image was collected in resolutions of 512×512 pixels. It is worth noting that there is no need, to our knowledge, of a force constant using the method suggested here.

For the force-volume mode, a V-shaped silicon nitride cantilever with integrated pyramidal tip (similar to tip 2 above) was used. The radius of curvature of the tip was ~ 20 nm, and was found by using the same method as above. The force constant was found to be 0.04 N/m by using the resonance shift method (built-in option of Nanoscope 5.12r4 software).

RESULTS AND DISCUSSION

Method of detection of the rigidity change with AFM

Rationale

A more traditional approach to measure rigidity of thin film would be to record the force-distance curves and derive the Young's modulus directly from the curves. To do that, however, one has to 1), collect enough statistics to take into account a possible inhomogeneity of the film; and 2), know the topography of the film. In the case of the gold film on the QCM sensor, the surface can be approximately described as flat-covered with spherical protrusions (Fig. 3). The formulas describing the interaction between the AFM tip and the surface are quite different if the AFM tip scans above the top of the spherical protrusion, or in the valley between the protrusions. To measure simultaneously the tip position and the geometry of the surface, one needs to use the AFM force-volume mode (25–27). However, this particular mode requires a much longer time than the regular mode of scanning. It also is quite limited in the size of area it can examine because it is limited to 64×64 pixels to record the image. In addition, the film on the surface of the QCM sensor is not ideal. One area can differ from another area on the surface quite dramatically. Therefore, one needs to repeat the force-volume measurements many times at different areas to collect enough statistical data. Finally, to get reliable contact in the force-volume mode, one needs to use force that might damage a soft molecular layer.

Here we describe the use of a novel technique of AFM scanning that is considerably faster and gentler to the sample, to qualitatively observe the change of rigidity of the protein film. Such an observation is needed, for example, when developing a new biosensor, where it is not known whether the presence of ligand influences the rigidity or not. The suggested technique of scanning is based on AFM tapping in liquids with small amplitudes. We previously used a technique to observe multilayer growth of liquid crystals with no destruction (23). Here we show that the suggested new technique requires only one tapping scan before and one scan after the addition of ligand. Both scans have to be taken on the same surface area to obtain reliable statistics of the rigidity change.

The time required to collect both required scans (512×512 pixels each) using our new method is $\sim$10 min. To collect comparable statistics in the traditional force-volume mode it would take $>$40 h ($\sim$40 min per 64-$\times$-64-pixel scan). It should be noted, however, that the amount of calculation time can be greater using the suggested method, due to the lack of customized software.

Theory

Here we show that the increase of rigidity, the Young's modulus, of the surface layer can be estimated using a relatively simple experimental method, which requires just two regular AFM scans, without special calibrations or measuring the forces. In this method, we scanned the immobilized protein on the surface and then the same area with ligand (glucose) added to obtain two topographical images of the surface. The change of rigidity of the surface layer can be found by using various indentation models. It is intuitively clear that the conclusion about either increase or decrease of the Young's modulus is independent of a specific model. To demonstrate the method, we will use the classical Hertzian model (see, e.g., (29)). The same conclusions about the rigidity can be obtained by using more sophisticated semiempirical multilayer models, reviewed in Kovalev et al. (22). However, to show it here is beyond the scope of this work.

We model the AFM tip-sample contact by two deformed spheres (Fig. 4). The deformation distance d (penetration) of two such spheres of radii R and R', which have different modulae E and E', is shown in Fig. 4.

The relation between the applied load force F, which induces the deformation, with deformation d, is given by the following formula (30):

$$d = F^{2/3}\left\{D^2\left[\frac{1}{R}+\frac{1}{R'}\right]\right\}^{1/3}, \tag{1}$$

where

$$D = \frac{3}{4}\left\{\frac{1-\nu'^2}{E'}+\frac{1-\nu^2}{E}\right\} \tag{2}$$

is a combination of the Young's modulus and the Poisson ratio ν and ν'.

It is a good approximation to consider the AFM tip as considerably more rigid than the sample surface. Hereafter, we put $E' \to \infty$ (let the AFM tip be the upper sphere). Furthermore, we will use $\nu = 0.5$, which is the case for incompressible materials. It should be noted that our conclusions do not

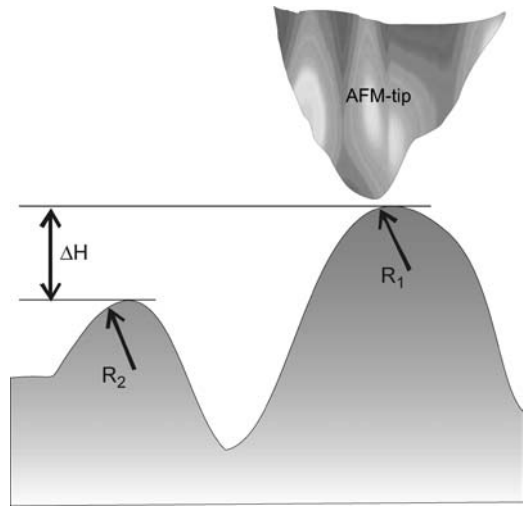

FIGURE 3 A configuration of an AFM tip and two spherical protrusions.

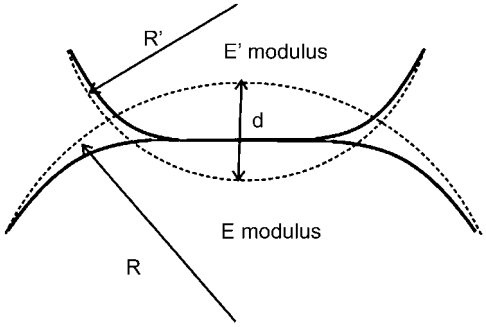

FIGURE 4 A scheme of the AFM tip-surface contact.

depend on the latter assumption. These two assumptions reduce Eqs. 1 and 2 to

$$d = F^{2/3}\left(\frac{3}{4}\right)^{4/3}\left\{\left(\frac{1}{E}\right)^{2}\left[\frac{1}{R}+\frac{1}{R'}\right]\right\}^{1/3}. \tag{3}$$

If the protrusion is not spherical, but elliptical, there is a simple modification of the above formula (30). In such a case, the radius factor $1/R + 1/R'$ is changed by an effective one, the geometrical average of the multiplication of two radius factors, $R_{\min}$ and $R_{\max}$, for both major axes of the ellipsoid:

$$\frac{1}{R_{\text{eff}}} = \sqrt{\left(\frac{1}{R_{\min}}+\frac{1}{R'}\right)\left(\frac{1}{R_{\max}}+\frac{1}{R'}\right)}. \tag{3a}$$

Let us now consider a case in which the AFM tip scans over two protrusions, of radii R_1 and R_2, which are covered by a layer that has rigidity E (Fig. 3). If scanning is done with the load force F, the AFM tip causes deformations d_1 and d_2 over the protrusions R_1 and R_2, (R_{eff1} and R_{eff2}) respectively. Here, we consider $R_{1,2} \gg d_{1,2}$, which corresponds to our experiment. Therefore, we will not consider the change of radius of the protrusions due to the film deformation. The height difference ΔH (see Fig. 3) as measured in the AFM scan is given by

$$\begin{aligned}\Delta H &= (h_1 - d_1) - (h_2 - d_2)\\ &= h_1 - h_2 + F^{2/3}\left(\frac{3}{4}\right)^{4/3}\left(\frac{1}{E}\right)^{2/3}\left\{\left(\frac{1}{R_{\text{eff2}}}\right)^{1/3} - \left(\frac{1}{R_{\text{eff1}}}\right)^{1/3}\right\},\end{aligned} \tag{4}$$

where h_1 and h_2 are the heights of the nondeformed protrusions.

If the material (film) rigidity changes, the height ΔH will have a different value. For example, as we demonstrate in this article, the protein film changes its rigidity if we add glucose. Scanning the same area with the AFM before and after adding glucose, we can measure the changes of height $\Delta H_{\text{no glucose}}$ and $\Delta H_{\text{with glucose}}$ between the same two protrusions. Subtracting these two values, and using Eq. 4, produces

$$\begin{aligned}\Delta &= \Delta H_{\text{no glucose}} - \Delta H_{\text{with glucose}}\\ &= F^{2/3}\left(\frac{3}{4}\right)^{4/3}\left(\left(\frac{1}{E_{\text{no glucose}}}\right)^{2/3} - \left(\frac{1}{E_{\text{with glucose}}}\right)^{2/3}\right)\\ &\quad\left\{\left(\frac{1}{R_{\text{eff2}}}\right)^{1/3} - \left(\frac{1}{R_{\text{eff1}}}\right)^{1/3}\right\},\end{aligned} \tag{5}$$

where $E_{\text{no glucose}}$ and $E_{\text{with glucose}}$ are the Young's moduli of the film in the absence and presence of glucose.

One can see that the difference Δ is an indicator of the film rigidity change after adding glucose. Because R_1 and R_2 can be directly measured from the AFM scans, the difference Δ gives an unambiguous answer based on the sign of the rigidity change. For example, as one can see from Eq. 5, if $E_{\text{no glucose}} < E_{\text{with glucose}}$, then the difference Δ is positive, provided $R_{\text{eff1}} > R_{\text{eff2}}$.

It should be noted that applying the above derivation to a film on a rigid surface, we assumed the deformation of the film to be small, and, as a result, the influence of a more rigid surface is negligible. Indeed, a more exact model (22) is needed if more quantitative results are required. However, using that more complex model here would not change the qualitative result.

There is one natural limitation to the usability of our new method, which occurs due to a possible change in long-range forces acting between the tip and surface. Because both scans should be collected while using the same force of interaction between the tip and surface, the load force is the same if and only if the tip-surface interaction is the same. If the addition of ligand alters the long-range force, it makes our method much more complicated. In our case, the use of buffer with 50 μM glucose as ligand in a buffer of 0.1 M ionic strength should not change possible long-range forces. In any case, the strongest component of the long-range forces, the electrostatic interaction, is shielded by the high ionic strength of the buffer (Debye length ~1 nm).

Another method of estimating the rigidity might be to observe the changes in surface roughness. Roughness depends on the variation of the surface heights. Looking at Eq. 4, which calculates such variations, one can see, however, that any change of rigidity can lead to either a decrease or an increase in roughness depending on the surface geometry. To make even a qualitative statement, one would need to calculate deformation of the surface at each point, which is impractical.

Experiment

To study the change of rigidity with AFM, two scans were taken, as described above. A representative scan without glucose using tip 1 is shown in Fig. 5 *a*. To exclude a possible simple removal of the protein film during scanning, three scans were executed. The last scan was recorded and used for further analysis. Glucose was added and the same region was scanned (Fig. 5 *b*). Despite some thermal drift, all features in

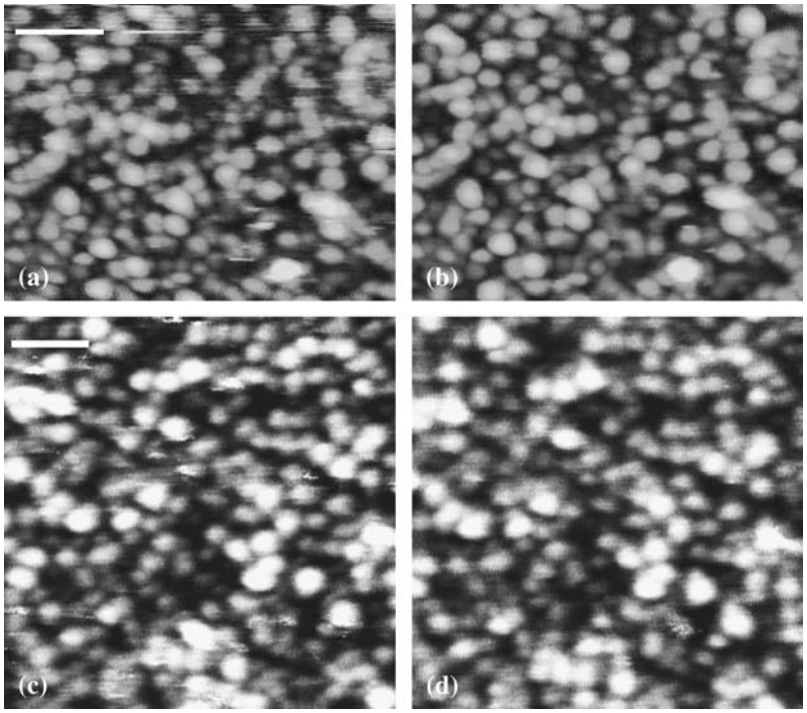

FIGURE 5 (*a*) AFM scan with tip 1 of an area of gold with the receptor GGRQ26C proteins attached. (*b*) Scan with tip 1 of the same area but with glucose added. (*c*) Scan with tip 2 of another area of gold with the receptor GGRQ26C proteins attached. (*d*) Scan of the area shown in *c* with glucose added. Scale bar, 200 nm.

the images can be easily identified. Fig. 5, *c* and *d*, shows the same type of images obtained with tip 2 before and after adding glucose, respectively.

One can see in Fig. 5 that relatively high noise in images *a* and *c* is gone in images *b* and *d*. This is a typical behavior when the film increases its toughness, and it is more durable. However, to exclude ambiguity of radius calculations in the noisy area, we did not use those areas in further calculations. Fig. 6 shows bearing analysis of depth distributions highlighting the changes in the film morphology before and after adding glucose. Each point on the curve shows the fraction of the film in the imaginary plane drawn at a corresponding depth below the topmost point of the surface. One can clearly see that there is a smaller number of highs (a slower increase of the histogram portion shown with an increase of depth near zero) before adding glucose. Comparing this result with Fig. 5, *a* and *c*, one can conclude that this is due to the higher amount of spiky noise, which almost disappears after adding glucose. We observe similar behavior with the calculation of roughness. After adding glucose, roughness drops from 1.63 nm (Fig. 5 *a*) to 1.47 nm (Fig. 5 *b*) and from 1.81 nm (Fig. 5 *c*) to 1.68 nm (Fig. 5 *d*).

To analyze the change of the Young's modulus, we measure the radii of the protrusions in Fig. 5 and the change of height, Δ, of formula 5. Fig. 7 shows an example of cross section of two protrusions before and after adding glucose. Because we need to find the radii of the protrusions and their relative height, it is worth processing the image through the low-pass filter. Random noise can be removed in this way. This fairly simple procedure should be watched, however, so as not to possibly change the data (heights and radii). The radii of curvature were found using SPIP software (Image-met, Copenhagen, Denmark). Then we need to find the effective radii (Eq. 3a). For example, for one protrusion we found $R_{\min} = 144 \pm 5$ nm and $R_{\max} = 232 \pm 8$ nm. Taking a tip radius of 20 nm, one gets $R_{\text{eff}} = 18.0 \pm 0.1$ nm. It should be noted that it is not an easy task to estimate the load force during the tapping scanning. Fortunately, it is not necessary to use the load force to find the rigidity change (see above). For our estimate, we use $F = 0.1$nN. This number comes from the fact that we were able to image liquid crystals (23) using similar tapping mode, whereas the crystal destruction starts at forces of $\sim$1 nN (21). Table 1 shows the effective radii and measured Δ, and the numerical results for

$$\left(\frac{1}{E_{\text{no glucose}}}\right)^{2/3} - \left(\frac{1}{E_{\text{with glucose}}}\right)^{2/3} = \frac{\Delta}{F^{2/3}(3/4)^{4/3}}\left(\left(\frac{1}{R_{\text{eff2}}}\right)^{1/3} - \left(\frac{1}{R_{\text{eff1}}}\right)^{1/3}\right)^{-1}, \qquad (6)$$

which we called the rigidity factor change (RFC). Histograms of these results are presented in Fig. 8. In these calculations, we choose to keep the definition of radii so that $R_1 > R_2$. Therefore, the positive factor (Eq. 6) corresponds to the increase of the Young's modulus of the film.

One can see from Fig. 8 that the film statistically increases its rigidity. The average increase is $+2 \times 10^{-4}$ Pa$^{-2/3}$ when using tip 1 (Fig. 5 *a*), and $+1 \times 10^{-4}$ Pa$^{-2/3}$ for tip 2 (Fig. 5 *b*). The observed decrease in some cases could probably be

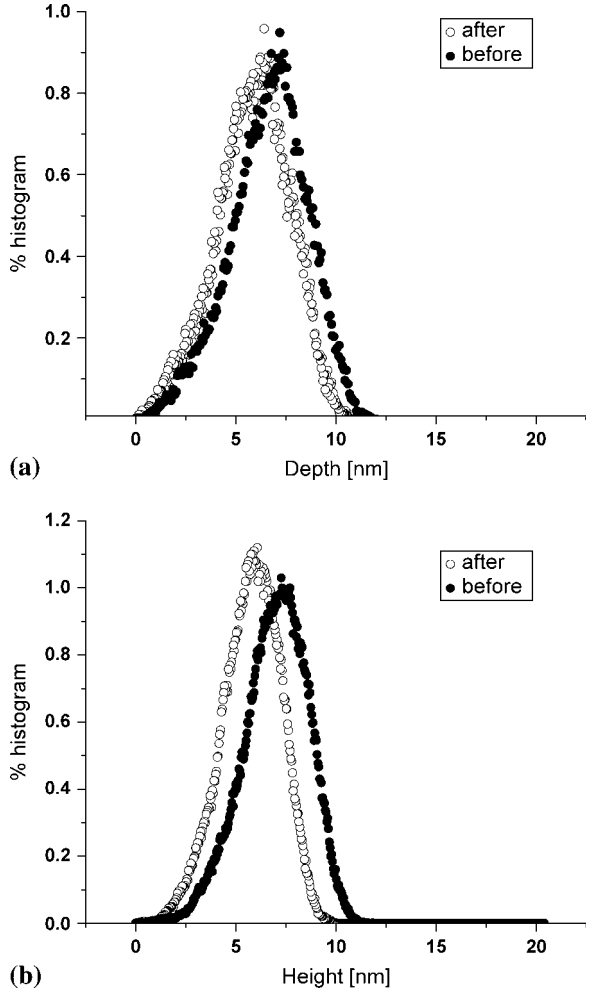

FIGURE 6 Bearing analysis of depth distributions highlighting the changes in the film morphology of the surfaces shown in (*a*) Fig. 5, *a* and *b*, and (*b*) Fig. 5, *c* and *d*, before and after adding glucose.

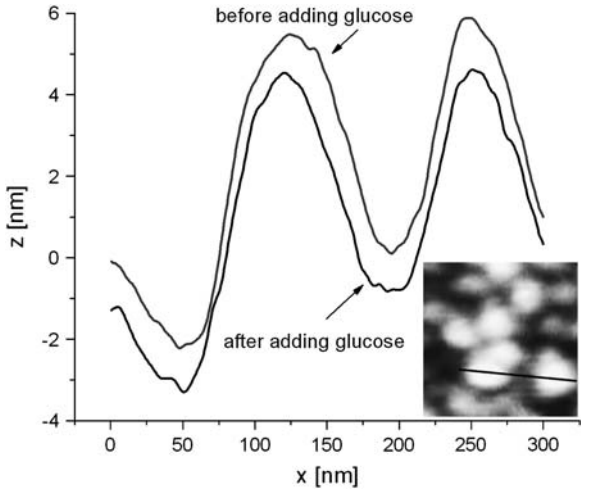

FIGURE 7 An example of a cross section of two protrusions before and after adding glucose. A small vertical shift is artificial, and introduced for better presentation as well as to stress the fact that the absolute vertical shift is meaningless in the AFM imaging. The inset shows the corresponding part of the AFM scan.

explained by irregularity of the film properties, or adsorption of additional layers after adding glucose. In some cases (~20%), we were not able to detect the height change because it was too small, below the sensitivity of the instrument. Those data are not plotted in Fig. 8.

One point should be made about the resolution and optimal scan size of the collected images. Because we need to access relatively small features, protrusions, it is worth having as much pixel resolution as possible. For the lateral size of the scan, it needs to be large enough to provide enough statistical data. We found that 1.5–2 μm is close to optimum with this type of surface feature.

Quantitative measurement of the Young's modulus with the force-volume mode

To validate our new method, we compared the above results with direct measurements of the Young's modulus by collecting the force curves in the force-volume mode. An integrated pyramidal tip was used in these measurements (similar to tip 2). Radius of curvature of the tip and the cantilever spring constant were measured as described in Materials and Methods. To analyze our data from the force-volume mode, we used the Hertzian model as described by Eqs. 1 and 2. Analysis of the force-volume data was done as follows. First, 20 to 30 force curves measured on the tops of the protrusions were averaged. Fig. 9 shows an example of three averaged force curves before and three after adding glucose. The procedure of finding the Young's modulus from this type of curve is described in detail elsewhere (27). Each average force curve was processed to calculate the Young's modulus versus penetration d by using Eq. 1. The results of the analysis of six measurements before and six after adding glucose are presented in Fig. 10. One can see an unambiguous change of the Young's modulus after adding glucose.

The increase of the rigidity with the tip penetration is expected due to approaching the much more rigid gold substrate. One can also see the change of thickness of the protein film. Although the thickness before adding glucose is ~6–7 nm, after adding glucose, the film becomes ~3–4 nm thick. This is shown chematically in Fig. 11.

It should be noted that the values of the Young's modulus and the film thickness obtained in this study are in good agreement with the values estimated by Carmon et al. (15) to explain the QCM data. It is also interesting to compare the results presented in Fig. 6 with the calculations used for the change of rigidity factor (Eq. 5). Assuming $F = 0.1$nN, $R_1 = 140$ nm, $R_2 = 50$ nm, and taking the Young's moduli $E_{\text{no glucose}} = 0.25\times10^6$Pa and $E_{\text{with glucose}} = 0.5\times10^6$Pa from Fig. 6, one can get $\Delta = 0.4$ nm. The experimental data corresponding to those radii show $\Delta = 0.6$–0.8 nm. This

TABLE 1 Measured effective radii, corresponding change of heights Δ, and the RFC

Tip 1			
R_{eff2}	R_{eff1}	Δ	RFC × 10^4
11.44889	18.63429	0.537	0.550076
9.046751	10.98104	0.62	1.406924
10.76164	11.31097	1.015	9.274668
10.29985	10.70296	0.89	10.37355
10.77813	11.16096	0.292	3.79837
11.41976	11.78241	−0.495	−7.32426
10.71443	10.93259	−0.204	−4.57475
11.26769	11.41268	0.323	11.59795
11.50015	11.69614	−0.409	−11.1952
11.00416	11.34787	0.258	3.832318
11.51539	11.90056	−0.579	−8.16543
10.90402	13.03524	0.505	1.320342
11.16213	11.61062	0.412	4.807746
11.0344	11.3727	−0.418	−6.32907
11.51705	11.71837	−0.106	−2.83098
11.64674	11.84337	0.442	12.26322
11.54577	11.70462	0.304	10.29863
11.28463	11.42394	0.226	8.460245
11.45903	11.57992	0.104	4.573301
11.23727	11.28092	0.103	12.17006
11.38066	11.52996	0.229	8.093789
11.3048	11.66168	0.239	3.545001
10.8151	11.59488	0.135	0.886496
11.23876	12.09226	−0.22	−1.39261
10.49318	11.55759	−0.33	−1.55279
9.921447	11.29183	–0.744	–2.57988
Tip 2			
R_{eff2}	R_{eff1}	Δ	RFC × 10^4
18.06	20.58	0.42	1.8
17.61	18.52	0.48	5.1
17.68	18.59	0.35	3.7
17.63	18.54	0.22	2.3
17.44	18.25	−1.04	−12.2
16.95	17.72	0.36	4.3
17.40	17.79	−0.43	−10.4
18.01	18.37	0.68	18.2
17.51	17.83	0.04	1.3
17.83	18.06	−0.42	−17.6
17.47	17.57	0.23	22.0
17.53	17.81	0.34	11.2
17.67	18.04	−0.54	−13.7
17.52	18.02	−0.83	−15.8
17.55	18.06	0.41	7.7
17.80	18.44	0.30	4.6
17.26	18.08	0.32	3.7
17.69	18.55	0.35	3.9
18.13	19.74	1.19	7.6
17.72	19.51	0.26	1.5
17.95	19.74	−0.33	−1.9
17.70	19.52	−1.39	−7.7
17.69	19.71	0.27	1.3
17.65	19.77	0.19	0.9
15.77	17.93	1.12	4.6
18.66	20.87	−0.66	−3.3
17.80	20.16	−0.45	−2.0
17.91	20.34	0.68	2.9
18.10	20.81	0.54	2.1

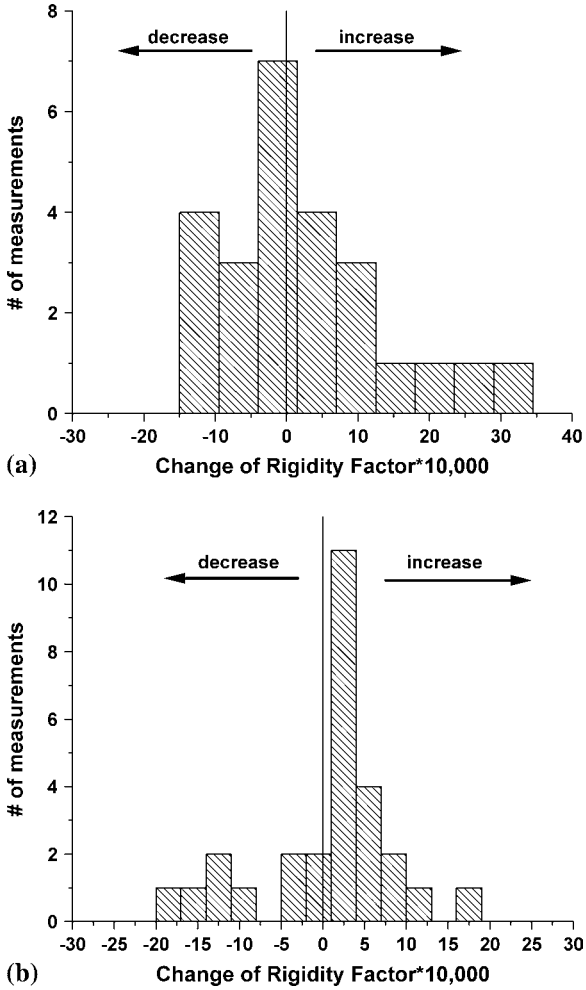

FIGURE 8 Histogram of the rigidity factor change calculated from Eq. 6. Positive values correspond to the increase and negative values to the decrease of the Young's modulus (rigidity) of the film. The average rigidity factor change is $+2 \times 10^{-4}$ $Pa^{-2/3}$ when using tip 1 (Fig. 5 *a*), and $+1 \times 10^{-4}$ $Pa^{-2/3}$ for tip 2 (Fig. 5 *b*), which corresponds to an overall increase of rigidity.

small discrepancy can be explained by using the Hertzian model, which is too simplified for quantitative analysis. Moreover, force F is not really known for the tapping mode. The use of a more sophisticated model for deformation of multilayered materials (22) gives $\Delta = 0.4$–0.6 nm for the same parameters as those used above. This shows consistency in both methods. To make the statement of consistency more convincing, let us note that there is some basic difference between these two methods. First, the rigidity change method is more statistically sound. The analysis in that method covers a considerably larger area, and a larger number of surface spherical protrusions. Second, in that method, the areas of study were the same before and after adding glucose, whereas they were different in the force-volume measurements. This will add more uncertainty to a direct comparison of the methods. In the force-volume method, the radii of gold

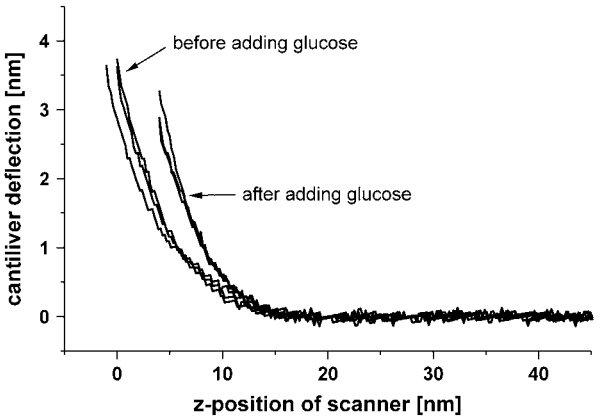

FIGURE 9 An example of three averaged force curves collected before and three after adding glucose. Raw data of the AFM cantilever deflection (in nanometers) versus z-position of the scanner are shown.

spherical protrusions were found with less precision because of the limited spatial resolution (limited number of pixels). Furthermore, we did not have the ability to exclude some ''noisy'' areas in the force-volume mode (it was not possible to detect with the limited number of pixels), as was possible using the other method. Finally, the force-volume method requires attaining considerably higher AFM tip-surface forces to observe reliable tip-surface contact. This can result in the possible destruction of the multilayered film, which could be responsible for the decrease in the film rigidity shown in Fig. 8. Thus, some quantitative discrepancy between these two methods is expected.

The measured increase of rigidity makes sense from a biochemical point of view. When glucose binds to the receptor, a large conformational change takes place and the glucose is buried deep in the interior of the protein. The overall

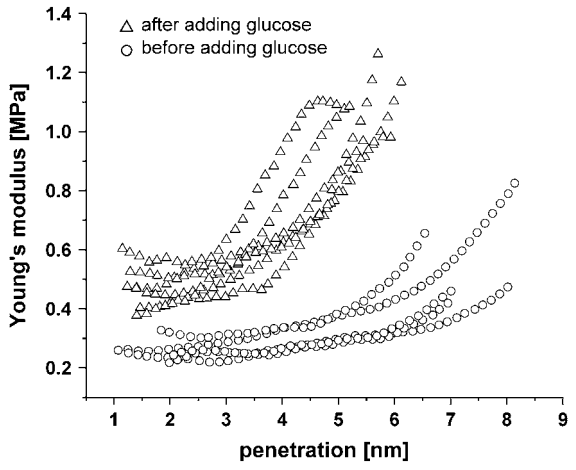

FIGURE 10 Dependence of the Young's modulus on penetration (deformation) of the AFM tip into the surface. Six curves before and six after adding glucose are presented.

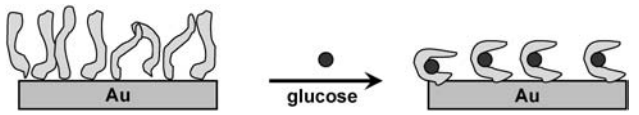

FIGURE 11 A schematic of spatial organization of GGRQ26C proteins before and after adding glucose.

surface of the protein does not change significantly and one would not expect a major change in chemical composition of the GGR-glucose complex from the unbound GGR. The glucose binding is through a large network of hydrogen bonds that do not change the ionic character of the protein in solution. Within the cavity, when the protein is open, there are hydrogen bonds to the water solution that encompasses the protein. When glucose binds to the cleft, the OH groups on the sugar molecule replace the hydrogen bonds to water (28). Several hydrogen bonds are formed between the two lobes of the protein as the hinge closes. This change in the protein upon glucose binding causes many secondary elements within the structure to change. These shifts are presumably responsible for the increase of rigidity and compactness of the protein, which have been measured here by AFM. The glucose is held within the interior by a network of hydrogen bonds that secures the two domains together, sequestering the ligand away from the solvent.

CONCLUSION

We studied mechanical behaviors of the protein film used for detection of glucose in a QCM-based biosensor. A receptor protein, GGRQ26C, was immobilized on the gold surface of the sensor. We found that the binding of glucose to the protein on the sensor surface resulted in the increase of rigidity of the film. A straightforward approach to measure rigidity of the thin protein film would be to record the force-distance curves and derive the Young's modulus directly from the curves. However, for a number of applications, such a method is impractical mostly due to its large time consumption. Here we developed a simple and substantially faster method based on taking scans of the surface with the atomic force microscope. The method allows one to detect a qualitative change of the rigidity of a molecular (protein) layer activated by ligand.

The AFM data described supports the reason for the large increase in the QCM frequency when glucose is bound to the receptor film (15) and can explain the biophysical mechanism of detection of glucose by piezoelectric biosensors. This is very important to the future development of such biosensors for small ligands. Since there are a host of receptors that undergo structural change when activated by ligand, AFM can play a key role in the development and/or optimization of biosensors based on rigidity changes in biomolecules.

We gratefully acknowledge funding for this work by grants from the National Science Foundation (CCR-0304143 and CTS-032968) to I.S. and L.A.L., and the New York State Office of Science, Technology, and Academic Research (NYSTAR-CAMP-33378) to I.S.

REFERENCES

1. Stock, A. M., and S. L. Mowbray. 1995. Bacterial chemotaxis: a field in motion. *Curr. Opin. Struct. Biol.* 6:744–751.
2. Blair, D. F. 1995. How bacteria sense and swim. *Annu. Rev. Microbiol.* 49:489–522.
3. Felder, C. B., R. C. Graul, A. Y. Lee, H. P. Merkle, and W. Sadee. 1999. The Venus flytrap of periplasmic binding proteins: an ancient protein module present in multiple drug receptors. *AAPS Pharm. Sci.* 1:E2.Review.1–22.
4. Mowbray, S. L., and M. O. Sandgren. 1998. Chemotaxis receptors: a progress report on structure and function. *J. Struct. Biol.* 124:257–275.
5. Salopek-Sondi, B., M. C. Skeels, D. Swartz, and L. A. Luck. 2003. Insight into the stability of the hydrophobic binding proteins of *Escherichia coli*: assessing the proteins for use as biosensors. *Proteins.* 53:273–281.
6. Salopek-Sondi, B., and L. A. Luck. 2002. ^{19}F NMR study of the leucine specific binding proteins of *E. coli*: mutagenesis and assignment of the fluorotryptophane labeled residues. *Protein Eng.* 15: 857–861.
7. Salins, L. L. E., R. A. Ware, C. M. Ensor, and S. Daunert. 2001. A novel reagentless sensing system for measuring glucose based on the galactose/glucose-binding protein. *Anal. Biochem.* 294:19–26.
8. Dwyer, M. A., and H. W. Hellinga. 2004. Periplasmic binding proteins: a versatile superfamily for protein engineering. *Curr. Opin. Struct. Biol.* 14:495–504.
9. Marvin, J. S., and H. W. Hellinga. 1998. Engineering biosensors by introducing fluorescent allosteric signal transducers: construction of a novel glucose sensor. *J. Am. Chem. Soc.* 120:7–11.
10. Hsieh, H. V., Z. A. Pfeiffer, T. J. Amiss, D. B. Sherman, and J. B. Pitner. 2004. Direct detection of glucose by surface plasmon resonance with bacterial glucose/galactose-binding protein. *Biosensors Bioelectron.* 19:253–260.
11. Vyas, N. K., M. N. Vyas, and F. A. Quiocho. 1988. Sugar and signal-tranducer binding sites of the *Escherichia coli* galactose chemoreceptor protein. *Science.* 242:1290–1295.
12. Careaga, C. L., and J. J. Falke. 1992. Thermal motions of surface α-helices in the D-galactose chemosensory receptor. Detection by disulfide trapping. *J. Mol. Biol.* 226:1219–1235.
13. Wang, J., K. S. Carmon, L. A. Luck, and I. I. Suni, 2005. Electrochemical impedance biosensor for glucose detection utilizing a periplasmic *E. coli* receptor protein. *Electrochem. Solid St.* 8:61–68.
14. Luck, L. A., M. J. Moravan, J. E. Garland, B. Salopek-Sondi, and D. Roy. 2003. Chemisorptions of bacterial receptors for hydrophobic amino acids and sugars on gold for biosensor applications: a surface plasmon resonance study of genetically engineered proteins. *Biosens. Bioelectron.* 19:249–259.
15. Carmon, K. S., R. E. Baltus, and L. A. Luck. 2004. A piezoelectric quartz crystal biosensor: the use of two single cysteine mutants of the periplasmic *E.coli* glucose/galactose receptor as target proteins for the detection of glucose. *Biochemistry.* 43:1429–1456.
16. Janshoff, A., H. J. Galla, and C. Steinam. 2000. Piezoelectric mass-sensing devices as biosensors—an alternative to optical biosensors? *Angew. Chem.* 39:4004–4032.
17. Marx, K. 2003. Quartz crystal microbalance: a useful tool for studying thin polymer films and complex biomolecular systems at the solution-surface interface. *Biomacromolecules.* 4:1099–1120.
18. Hook, F., and B. Kasemo. 2001. Variations in coupled water, viscoelastic properties, and film thickness of a Mefp-1 protein film during adsorption and cross-linking: a quartz crystal microbalance with dissipation monitoring, ellipsometry, and surface plasmon resonance Study. *Anal. Chem.* 73:5796–5804.
19. Binnig, G., C. F. Quate, and C. Gerber. 1986. Atomic force microscope. *Phys. Rev. Lett.* 56:930–933.
20. Sokolov, I. Y., and G. S. Henderson. 2000. Atomic resolution imaging using the electric double layer technique: friction vs. height contrast mechanisms. *Appl. Surf. Sci.* 157:302–307.
21. Sokolov, I. Y. 2003. Pseudo-non-contact mode: why it can give true atomic resolution. *Appl. Surf. Sci.* 210:37–42.
22. Kovalev, A., H. Shulha, M. Lemieux, N. Myshkin, and V. V. Tsukruk. 2004. Nanomechanical probing of layered nanoscale polymer films with atomic force microscopy. *J. Mater. Res.* 19:716–728.
23. Sokolov, I., H. Yang, G. A. Ozin, and G. S. Henderson. 1997. Beyond the hemicylindrical micellar monolayer on graphite: AFM evidence for a lyotropic liquid crystal film. *Adv. Mater.* 9:917–921.
24. Tsukruk, V. V., V. V. Gorbunov, Z. Huang, and S. A. Chizhik. 2000. Dynamic microprobing of viscoelastic polymer properties. *Polymer Intern.* 5:441–447.
25. A-Hassan, E., W. F. Heinz, M. D. Antonik, N. P. D'Costa, S. Nageswaran, C. A. Schoenenberger, and J. H. Hoh. 1998 Relative microelastic mapping of living cells by atomic force microscopy. *Biophys. J.* 74:1564–1578.
26. Hoh, J. H., and C. A. Schoenenberger. 1994. Surface morphology and mechanical properties of MDCK monolayers by atomic force microscopy. *J. Cell Sci.* 107:1105–1114.
27. Berdyyeva, T. K., C. D. Woodworth, and I. Sokolov. 2005. Human epithelial cells increase their rigidity with ageing in-vitro: direct measurements. *Phys. Med. Biol.* 50:81–92.
28. Luck, L. A. 1995. ^{19}F NMR Studies of fluorinated sugars binding to the glucose and galactose receptor protein. *In* Techniques in Protein Chemistry VI. J. W. Crabb, editor. Academic Press, San Diego. 487–494.
29. Landau, L. D., and E. M. Lifshitz. 1986. Theory of Elasticity: Butterworth-Heinemann, Oxford University Press, Oxford, UK.
30. Johnson, K. L. 1985. Contact Mechanics. Cambridge University Press, Cambridge, UK.